3D-ambient noise surface wave tomography of Fogo volcano, Cape Verde

Joana Carvalho[a,*], Graça Silveira[a,b], Stéphanie Dumont[a,c], Ricardo Ramalho[d,e,f]

[a] Universidade de Lisboa, Faculdade de Ciências, Instituto Dom Luiz, Lisboa, Portugal.

[b] Instituto Superior de Engenharia de Lisboa (ISEL), Lisboa, Portugal.

[c] Instituto Dom Luiz (IDL), Universidade da Beira Interior, Covilhã, Portugal.

[d] Universidade de Lisboa, Faculdade de Ciências, Instituto Dom Luiz and Departamento de Geologia, Lisboa, Portugal.

[e] School of Earth and Environmental Sciences, Cardiff University, Park Place, Cardiff, CF10 3AT, United Kingdom.

[f] Lamont-Doherty Earth Observatory, Columbia University, Comer Geochemistry Building, PO Box 1000, Palisades, NY10964-8000, USA.

* Corresponding author: j.filipa.carvalho@gmail.com

Abstract:

Fogo volcano belongs to the Cape Verde Archipelago, and it is one of the most active volcanoes in the Atlantic Ocean, which most recent eruption occurred from November 2014 to February 2015. We analyzed ambient seismic noise recordings of three different networks deployed in the island, totalizing 14 seismic stations, to derive a crustal 3D shear-wave crustal velocity model of the volcano. Through the phase cross-correlation technique followed by a time-domain phase weighted stack, we were able to measure Rayleigh wave group-velocity dispersion measurements in the period range from 1.0 to 10 s. These dispersion measurements were used to invert for 2D group velocity maps at selected periods, and then inverted to produce a 3D shear-wave velocity model of the island. The tomographic model shows three velocity domains. First, an asymmetric upper layer, above 5–6 km of depth, with lower velocities concentrated in the northeastern sector of the island and a clear higher-velocity horizontal body at 3–4 km of depth in the southwestern sector of the island; the spatial correlation between these two velocity zones and the Galinheiros normal fault suggests a genetic link between the high velocities and long-term surface deformation, which we related to sill intrusions between 3 to 4.5 km depth, beneath the southwestern sector of the island. Second, a marked higher-velocity horizontal layer in between 5–6 km and 8–9 km, interpreted as the seismic expression of pervasive sill and laccolith intrusions, now cooled, beneath the volcanic edifice and within the underlying oceanic crust. Third, a lower velocity layer below 8–9 km of depth, more pronounced beneath the northeastern sector, which could be explained by a hotter and possibly melt-rich zone beneath the volcano or a significantly altered/serpentinized crust. Finally, our study also confirms that Fogo lacks any sizable magma chambers (ancient or recent) within the volcanic edifice, in agreement with other geophysical and petrological studies. These observations demonstrate that 3D-ambient noise Rayleigh wave tomography is a powerful tool to image the crustal and upper mantle structure beneath volcanic islands, as shown here for Fogo volcano.

Keywords: Cape Verde, Fogo volcano, Ambient seismic noise, Volcano tomography, Sill intrusions

1. Introduction

Fogo, a volcanic island located in the southwestern part of Cape Verde Archipelago (Fig. 1), is an active and populated intraplate volcano. The archipelago started to rise approximately 22 Ma but most of the islands formed in the last 16 Ma. Fogo is one of the most recent islands (~4 Ma; Ramalho, 2010a). At least three islands are considered to be volcanically active (Santo Antão, Fogo and Brava; e.g. Faria and Fonseca, 2014) but only Fogo had post-settlement eruptions. The last eruption started in November 2014 and lasted until February 2015.

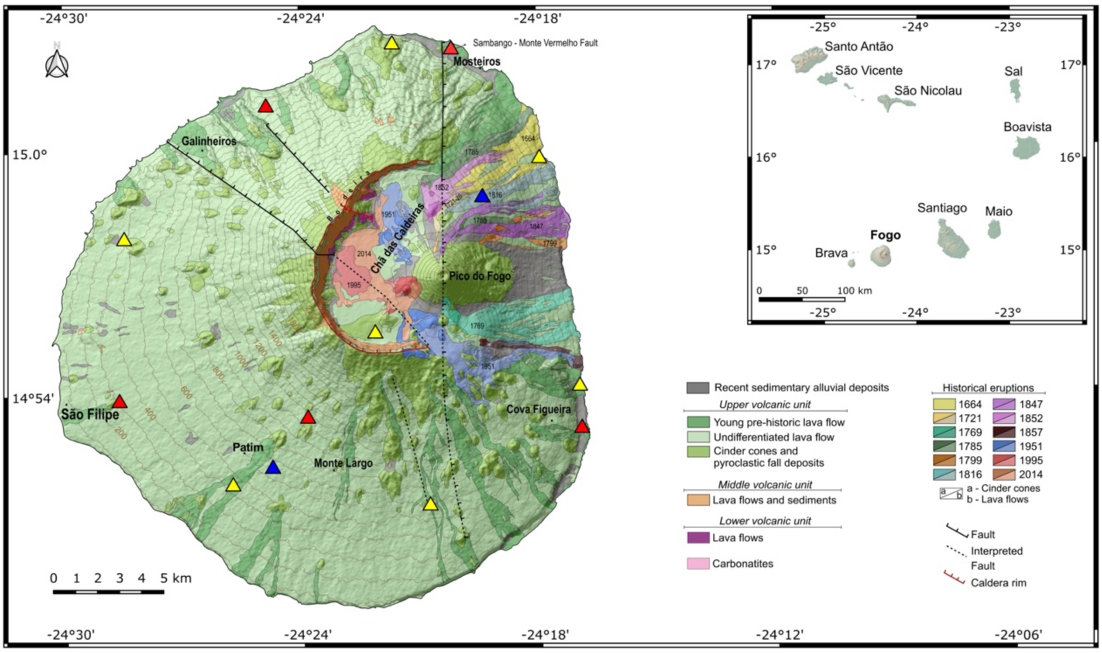

Figure 1: Top right: Geographic distribution of the Cape Verde islands. Left: Geological map of the island of Fogo (adapted from Martinez-Moreno et al., 2018) and some of the historical eruptions. The triangles represent the seismic stations used in this study. The different colors correspond to different seismic networks – Blue: YW; Red: 9A; Yellow: C4G. Topography of Fogo Island corresponds to digital elevation model at 1:5000 scale (UCCP/MAHOT, 2010).

Cape Verde has been the subject of several seismic studies, at different scales, with the aim of gaining insight on the archipelago's structure. Large-scale tomographic studies (e.g. French and Romanowicz, 2014; Montelli et al., 2006) have shown low-velocity anomalies in the lower mantle, in agreement with the presence of a mantle plume. Regional shear-wave velocity (Vs) models obtained from global observations of surface and shear waves (e.g. Schaeffer and Lebedev, 2015; Celli et al., 2020) display low-velocities in the asthenosphere.

The deployment of temporary seismic networks across the islands favored the local studies. Using different approaches, Helffrich et al. (2010) and Vinnik et al. (2012) inferred the thickness of the mantle transition zone beneath Cape Verde. Carvalho et al. (2019b) provided an average shear-wave velocity model for the Cape Verde region, suggesting the presence of a low-velocity zone at the asthenosphere depth. Liu and Zhao in 2014 and, more recently in 2021 presented a local tomographic model which brought new light on the deep structure of Cape Verde. The authors suggested not only the existence of a plume, but also its location beneath the Fogo Island. Recently, the first 3D shear-wave velocity model for the Cape Verde crust and uppermost mantle was obtained by Carvalho et al. (2022) and suggests low-velocity anomalies beneath Fogo and surrounding area as well. Whilst seismic studies focusing on the archipelago are relatively common, the same cannot be told about the individual islands. Fogo volcano, in particular, has been studied from different perspectives: geological and geochemical (e.g. Klügel et al., 2020; Mata et al., 2017; Melián et al., 2021), magnetotelluric (Martínez-Moreno et al., 2018), eruptive activity (González et al., 2015; Dumont et al., 2021), volcanic hazard and monitoring (e.g. Faria and Fonseca, 2014; Jenkins et al., 2017; Cappello et al., 2016; Leva et al., 2019); the island, however, still lacks a detailed characterization of its seismic structure. The primary goal of this study is to constrain, for the first time, a Vs model for Fogo volcano and its underlying crust.

Seismic tomography has proven to be a powerful tool to determine the seismic velocity structure of volcanoes (e.g. Brenguier et al., 2007; Jeddi et al., 2017; Obermann et al., 2016; Stankiewicz et al., 2010). The energy necessary to perform such tomographic studies in volcanic environments can be obtained from seismicity in the vicinity of the edifice (e.g Jaxybulatov et al., 2011), by active seismic sources (e.g. Tanaka et al., 2002) or by ambient seismic noise (e.g. Benediktsdóttir et al., 2017; Obermann et al., 2016). Ambient noise tomography is based on the validated assumption that the cross-correlation functions of a pair of recordings can be used to retrieve the Green's functions between two seismic stations, where one is the receiver and the other acts like a source (e.g. Campillo and Paul, 2003; Shapiro and Campillo, 2004). Over the last two decades, ambient noise tomography has been widely applied for imaging the Earth's structure at local, regional, continental, and even global scales (Carvalho et al., 2022 and references therein). The growing popularity of this technique is largely due to its advantages when compared to other tomographic techniques: it is independent of the occurrence of earthquakes or explosions, and it allows the imaging of regions where the resolution is only dependent on the network scheme. Moreover, at short periods, it is particularly difficult to obtain good surface wave dispersion measurements on waveforms resultant from earthquakes, due to attenuation and scattering. In these situations, it is especially useful to image the Earth structure with waveforms retrieved from ambient noise cross-correlations.

In this study, we use 14 seismic stations from three different temporary seismic networks deployed on Fogo Island (Fig. 1). After retrieving the Rayleigh wave Green's functions between each station pair of the same network, from ambient noise phase cross-correlation (PCC) functions and time-domain phase weighted stack (tf-PWS) (Schimmel et al., 2011), we measured the group-velocity dispersion curves (Herrmann and Ammon, 2002) and performed a 2D group velocity tomography (Rawlinson and Sambridge, 2005). Next, a grid was selected to invert, as a function of depth, for a 1D shear-wave velocity model at each node (Herrmann, 2013) and thus obtaining a 3D shear-wave velocity model for the crustal structure of Fogo Island in which the main seismic wave velocity anomalies were identified and discussed in the context of the local geology, geomorphology and petrology.

2. Geological setting

2.1. Cape Verde Archipelago and Fogo Island

Cape Verde is an intraplate oceanic group of 10 islands and some islets, located approximately 560 km away from the Senegal coast, Africa, in the Atlantic Ocean [14°–18° N and 22°–26° W] (Fig. 1), which stands as a surface manifestation of hotspot-driven volcanic activity associated with the bathymetric swell forming the Cape Verde Rise (Ramalho et al., 2010a). The islands are arranged in a west-facing horseshoe shape, with two diverging chains. Older islands are located to the east and younger islands to the northwest and southwest (Samrock et al., 2019).

The volcanic activity is thought to have started during the Late Oligocene/Early Miocene and extended into the Holocene (Torres et al., 2010), as suggested by the age of the oldest exposed lavas in the archipelago. Historical eruptions (<500 years) are unknown except in Fogo, which latest eruption occurred in 2014-2015 (e.g. Mata et al., 2017).

Fogo is one of the youngest islands of the archipelago, with the older exposed lava flows corresponding to ~212 ka (Marques et al., 2019). The volcanic edifice we see today, however, was possibly built over the eroded remains of an older volcanic edifice dated of 5.1 to 3.2 Ma (Bernard-Griffiths et al., 1975). Fogo island is topped by an 8-km wide depression – Chã das Caldeiras – which is bordered by a subvertical escarpment, the Bordeira, of up to 1 km high, forming a horseshoe open to the east (Fig. 1). Slightly off centered of Chã das Caldeiras stands Pico do Fogo, a stratovolcano representing the center of the current volcanic activity.

Several tectonic structures have also been identified on Fogo Island and were tentatively correlated with volcanic activity. In addition to the diffuse rift zones defined by Day et al. (1999) and Foeken et al. (2009), Brum da Silveira et al. (1997a,b) and Torres et al. (1998) identified and characterized several faults, volcanic and tectonic lineaments, some of which exhibit a clear morphological expression. Of these, one of the most noteworthy is the Galinheiros Fault (Figs. 1 and 2), a NE-SW normal fault that cuts diagonally across the island and is well exposed at the Bordeira wall south of Monte Amarelo spur (Torres et al., 1998).

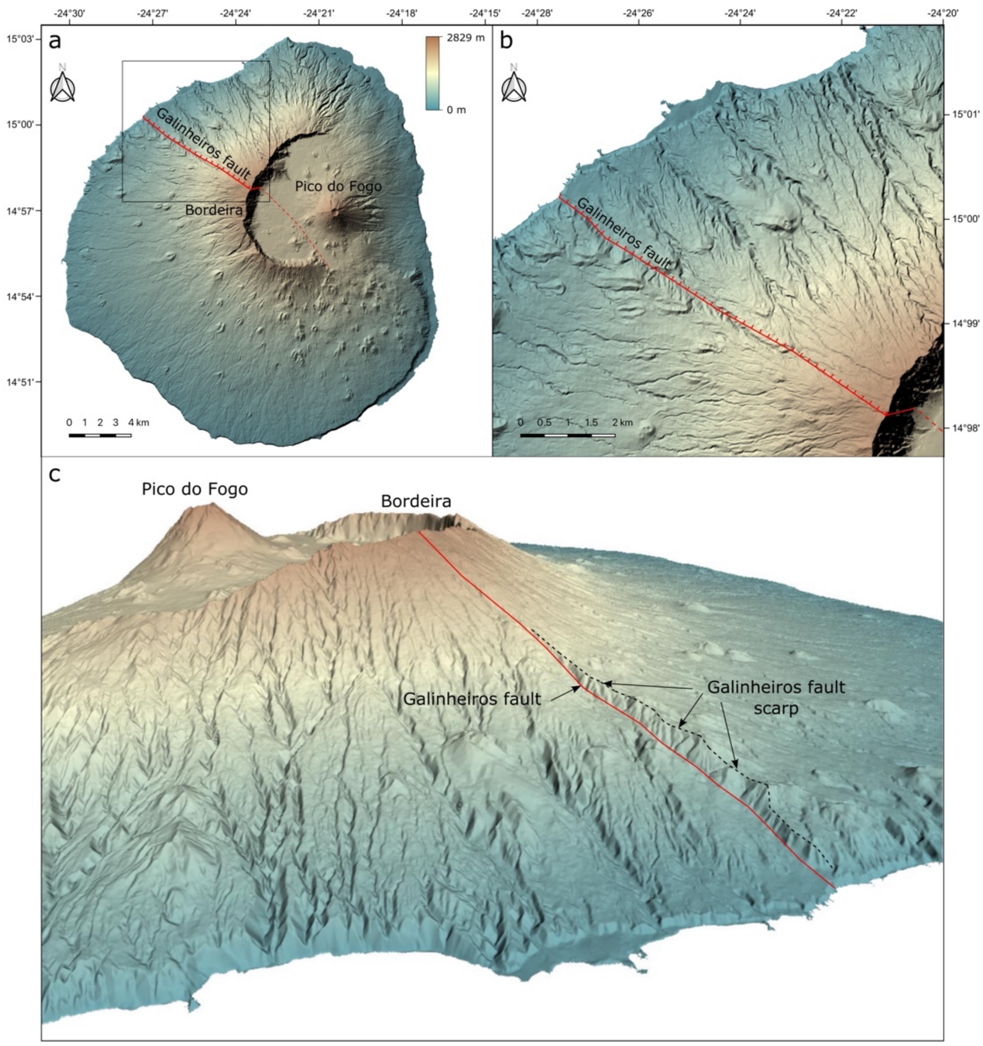

Figure 2: a) Digital elevation model of Fogo Island showing the location of the Galinheiros Fault. b) Zoom on the northern sector of the fault. c) 3D view (looking SE) of the north-western slope of Fogo, showing the scarp of the Galinheiros Fault, which exhibits >150 m of an apparent vertical displacement at its highest point. Topography of Fogo corresponds to digital elevation model at 1:5000 scale (UCCP/MAHOT, 2010).

This fault exhibits a maximum surface vertical displacement of >150 m, in its northern sector (to the south the fault is buried by recent lava flows), with the north-eastern half of the island downthrown relatively to its southwestern half. This geometry thus suggests either uplift of the south-western sector or subsidence of the north-eastern one, on account of a yet enigmatic mechanism.

2.2. Fogo volcano

Fogo volcano presently stands approximately 7 km above the surrounding seafloor, and morphologically exhibits a somma-vesuvius type association, with a younger stratovolcano (Pico do Fogo) which has been active over the last ~40 kyrs and developed on top of an older collapsed volcanic edifice (Monte Amarelo, Fig. 1) (Ribeiro, 1960; Brum da Silveira, 1997a,b; Day et al., 1999; Mata et al., 2017). Prior to the formation of Chã das Caldeiras, Monte Amarelo shield volcano covered most of the island, representing an area of approximately 475 km^2. Recent observations suggest that Chã das Caldeiras was formed by a combination of central subsidence triggered by caldera-forming large explosive eruptions followed by a large gravitational flank collapse possibly also ensuing in smaller, more recent gravitational collapses (Cornu et al., 2021). The age of the main collapse is now well bracketed at ~68 ka by K-Ar geochronology along Bordeira's volcanic succession (Cornu et al., 2021), which is in very good agreement with ^{3}He cosmogenic ages of 65–84 ka determined by Ramalho et al. (2015a) on megaclasts found at the adjacent Santiago Island, transported by the tsunami that resulted from the collapse. Subsequently to the lateral collapse, renewed volcanic activity resulted in the construction of the almost perfect conical stratovolcano of Pico do Fogo, presently reaching a height of 2829 m above present-day sea level.

Recent eruptions mostly took place at the periphery of the volcano, in its lower flanks (Carracedo et al., 2015; Worsley, 2015) (Fig. 1). Approximately 30 eruptions were reported since the discovery of the archipelago in 1500 CE, making Fogo one of the most active volcanoes of the Atlantic region. The most recent eruptions of 1995 and 2014-2015, afforded the opportunity to record geophysical, geological and geochemical data before, during and after the eruptions. Gathering such amount of data resulted in numerous studies that greatly advanced our knowledge of the volcano, including its magma source and its plumbing system (e.g. Munhá et al., 1997; Heleno da Silva et al., 1999; Amelung and Day, 2002; Hildner et al., 2011, Worsley, 2015; González et al., 2015; Cappello et al., 2016; Mata et al., 2017; Leva et al., 2019; Klügel et al., 2020; Dumont et al., 2021; Alonso et al., 2021). Modelling and geochemical studies have shown that major events like large flank collapses at oceanic islands volcanoes can strongly affect their entire magma plumbing system by disarranging the thermal and mechanical equilibrium of the volcano edifice (Maccaferri et al., 2017; Cornu et al., 2021). If a shallow magma chamber ever existed in Fogo volcano it was probably destroyed by the volcanic and gravitational collapses that gave origin to Chã das Caldeiras. Effectively, there is no evidence for a sustained crustal magma chamber, since neither geophysical observations (Amelung and Day, 2002; González et al.,

2015) nor geochemical data have allowed the identification of such a structure, only transient magma stalling at shallow depths was identified (Hildner at al., 2012; Mata et. al., 2017). In fact, Hildner et al. (2012) suggest that there is no petrological evidence for shallow magma chambers in the crust, neither prior nor after the Monte Amarelo flank collapse. Furthermore, these authors conclude that despite the high rates of magma supply, the lack of a persistent shallow magma chamber can be a consequence of the cold Mesozoic crust and thick lithosphere beneath Fogo.

The sparse volcano-tectonic seismicity associated with Fogo eruptions, and the almost absence of such events in between eruptions, reinforce the idea of a deeper magma reservoir (Fonseca et al., 2013 and references therein), which is further confirmed by studies on gas emitted from the summit caldera (Aiuppa et al., 2020; Mélian et al., 2021; Alonso et al., 2021). Interestingly, however, Leva et al. (2019) located a cluster of approximately 20 mantle earthquakes beneath the southern part of Fogo volcano, at depths ranging from 38 to 44 km. According to these authors, these earthquakes were probably triggered by fracturing associated with magma injection (i.e. intrusive activity) in the upper mantle. More recently, Leva et al. (2021) using three arrays, two of them deployed on Fogo, analyzed the seismic activity in Fogo and Brava region. On Fogo, the authors mainly found hybrid events, which are events with a transition from high to low frequencies and without clear S-phase. Without any 3D velocity model available for the island, the authors located the events through a time-domain multi-array analysis, which is independent of velocity models. These hybrid events were shallow and located in the north-western part of the collapse scar of Fogo and on top of the Bordeira escarpment. An accurate and precise depth determination for the foci of these events, however, requires a high-resolution 3D velocity model.

3. Seismic networks and data pre-processing

This study is based on data from 14 broadband seismic stations, which are divided in three different temporary networks, YW (2002-2004) (Lodge and Helffrich, 2006); 9A (2007-2008) (Weber et al., 2007) and C4G (2014-2015) (Fig.1). This last network was temporarily deployed by the Collaboratory for Geosciences (C4G) consortium, quickly after the 2014-2015 eruption started (Dumont et al., 2021) and only operated between December 2014 and January 2015. As this network has no official code attributed, herein it will be named C4G network. A detailed description of each seismic network and respective sensors is presented on Table 1 of the supplementary material.

For each station, continuous vertical-component seismic records were initially cut into 1-hr length files and decimated from the original sampling rates of 100 Hz (9A and C4G) and 50 Hz (YW) down to 10 Hz, in order to reduce the computation time consuming. The instrument response was removed to convert each record to ground velocity and the seismograms were then band-pass filtered in the 0.1 – 2.0 Hz frequency band. The pre-processing steps were accomplished using the Seismic Analysis Code (SAC; Goldstein and Snoke, 2005).

4. Methodology

4.1. Empirical Green's functions retrieval and stacking

For all possible inter-station paths among the same network, we computed 1-hour length cross-correlations of the vertical component through the phase cross-correlation technique (PCC; Schimmel 1999). PCC is amplitude unbiased and therefore does not require time-domain normalization to remove unwanted signals, such as earthquakes or volcanic tremors. From 32 station pairs, we have obtained 62518 hourly cross-correlations (31505 from 9A network, 28505 from YW network and 2958 from C4G network). The EGFs were then obtained by applying the time-frequency domain phase-weighted stack (tf-PWS; Schimmel et al., 2011) for the entire recording period of each network. The tf-PWS was developed with the purpose of improving the signal-to-noise ratio as it emphasizes the coherent signal and mitigates the incoherent one. Several authors have shown that applying together the PCC and tf-PWS considerably improves the signal and results in more robust group-velocity measurements (e.g. Acevedo et al., 2019; Corela et al., 2017; Hable et al., 2019; Haned et al., 2016; Nuñez et al., 2019; Sánchez-Pastor et al., 2021, Silveira et al., 2022, Carvalho et al., 2022). In Fig. 3 we present all the computed EGFs (32 in total) as a function of inter-station distance and lag time. The corresponding inter-station paths are represented on top of the map of the island. Some EGFs are dominated by low frequency content (9A and YW networks), whereas others show more high-frequency content (C4G network). However, the C4G network data contribution to this study is much less than the two other networks. Fig. S1 of the supplementary material shows some EGFs examples with multiple frequency bands in order to better understand the data distribution at different frequencies. As far as we only considered the vertical component for this study, the surface waves emerging from the background noise are mainly short-period Rayleigh-waves.

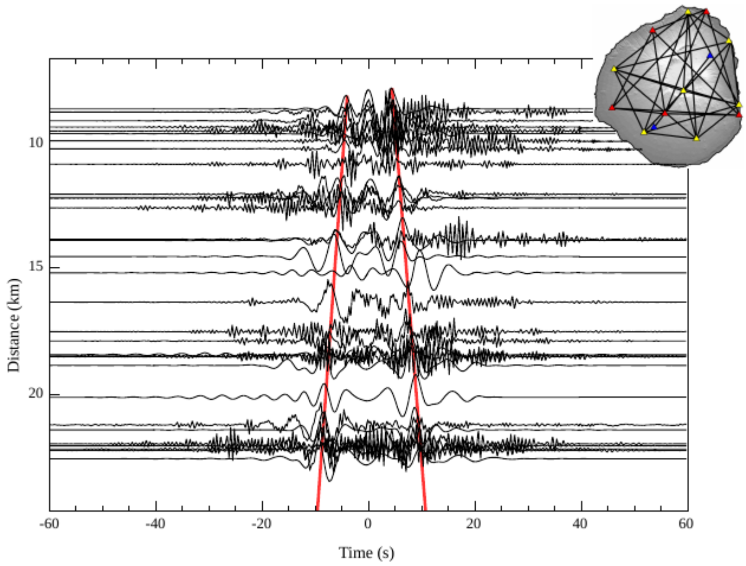

Figure 3: Record section showing the empirical Green's functions for all the station pairs available plotted according to the inter-station distances. The red lines indicate the 1.8 km/s moveout. On the top right corner, we present the map of the island with the seismic stations colored according to the network (Blue: YW; Red: 9A; Yellow: C4G) and all possible inter-station paths between stations of the same network.

4.2. Group velocity dispersion curves

Several techniques, semi- or fully automatically, exist to decompose the EGFs in the time-frequency domain and thus obtain the dispersion curves of the Rayleigh waves (Levshin et al., 1989, Herrmann and Ammon, 2004; Yao et al., 2006, Schimmel et al., 2017). In this study we applied the multiple filtering analysis (MFA) of Dziewonski et al. (1969), as implemented by Herrmann and Ammon (2004) in the package *Computer Programs in Seismology* (Herrmann, 2013). We computed time-frequency energy diagrams in the period range 1–10 s, under the program *do_mft,* to measure the Rayleigh-wave group velocity dispersion curves. The energy diagram is a surface defined by the envelopes of the trace narrow band-filtered around each centered frequency. For each frequency, the Rayleigh wave fundamental mode group travel time was automatically obtained from the maximum of the envelope and then manually validated. After processing all files, the selected curves were visually inspected. In case of detection of inconsistent measurements, these were discarded. Fig. S2 shows three examples (one path for each seismic network) of the picked dispersion measurements and in Fig. 4 we show all the dispersion curves calculated (colored dots) and the outliers, which were removed and not considered in further computations (red circles). The different colors represent the different seismic networks.

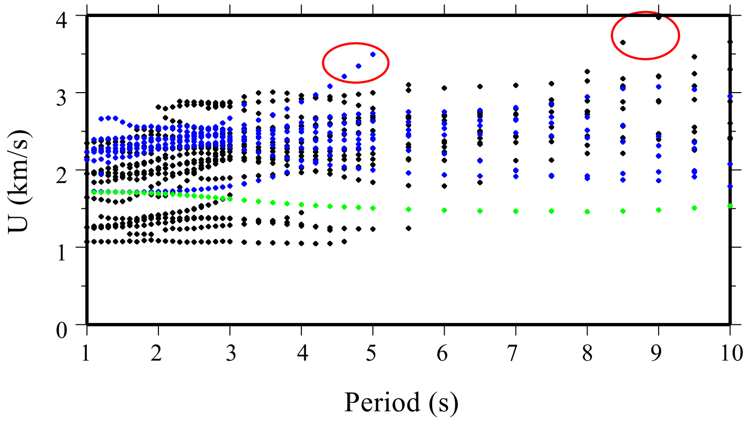

Figure 4: Rayleigh wave group-velocity measurements from C4G (black dots), 9A (blue dots) and YW (green dots) seismic networks. The red circles highlight the measurements considered outliers and which were removed and not accounted in further computations.

5. Rayleigh-wave Tomography and Depth Inversion

5.1. Resolution tests

Before proceeding to the inversion with real data, it is important to evaluate the array capability to solve the velocity structure, at different periods, through the checkerboard test. Several synthetic checkerboards were performed, with different grid spacings (10 x 10, 12 x 12 and 14 x 14 grid points), in order to decide the final grid dimension. Fig. 5 shows input synthetic checkerboard models (top panel) and the recovered anomalies (bottom panel), for each grid-cell size, computed with the Fast Marching Surface Tomography package (FMST; Rawlinson and Sambridge, 2005).

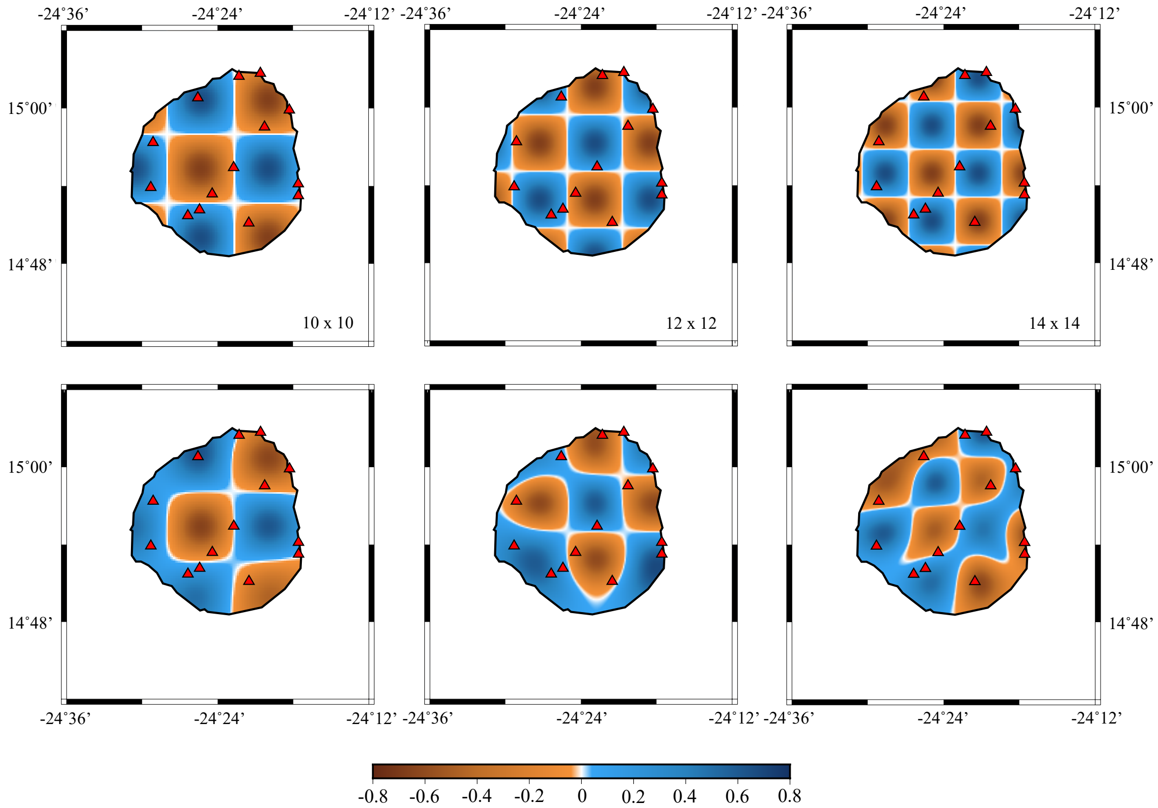

Figure 5: Synthetic input checkerboard (top panel) and the recovered anomalies (bottom panel) for different grid cell-sizes as indicated in the lower right corner of the top panel. Red triangles represent the seismic stations.

A grid built with less grid points results into bigger cell sizes. Considering the dimension of the island (~ 476 km^2), cells as big as the ones represented in the 10 x 10 grid will not allow the recovery of small features. On the other hand, when increasing the number of grid points, and so decreasing the cell size, the anomalies start to appear elongated towards NE-SW (smearing), which indicates that the 14 x 14 grid it is not suitable to solve the velocity structure. We consider the 12 x 12 grid presents the appropriate grid cells size to recover the anomalies with enough resolution to draw the main features. Gaussian random noise with a standard deviation of 0.3 was added to the synthetic data in order to simulate the observational data.

Because the number of inter-station paths does not change considerably in all periods (Fig. S3, supplementary material), the recovered anomalies are, in general, well resolved and consistent for all the considered periods (Fig. S4, supplementary material).

5.2. 2-D Rayleigh-wave tomographic inversion

In order to obtain the 2D velocity maps, for each period, from the Rayleigh wave group velocity dispersion curves we applied the FMST inversion approach. FMST follows a non-linear inversion scheme that relies on two steps: 1) prediction of travel-times (forward problem) and 2) adjustment of the model parameters that best match the data, using regularization constrains (inverse problem). The 2D model is parametrized with a grid with 12 x 12 = 144 velocity nodes, which are regularly spaced by approximately 0.036 degrees in latitude and longitude. The initial model for the inversion has a constant velocity that is taken as the mean group velocity for each period. The regularization parameters (smoothing (η) and damping (ε)), which ensure that the resulting model satisfies the data well and yet does not diverge too much from the initial model, were tested trough repeated iterations of the L-shaped trade-off curves for different values (Fig. S5 of supplementary material), as in Rawlinson et al. (2006). Starting from $\varepsilon = 0$, and fixing the $\eta = 1.0$, the damping was allowed to progressively vary while calculating the data residuals (RMS) and the model variance. We considered that $\varepsilon = 0.2$ represents a good adjustment between the RMS and the model variance. The same procedure was applied to determine the smoothing parameter, this time by fixing the $\varepsilon = 0.2$, and varying the smoothing from 0 to 20. The optimal value between data misfit (RMS) and model roughness is $\eta = 1.0$.

We performed tomographic inversions of the group-velocity measurements for 29 periods between 1.2 and 9.5 s (with steps of 0.2 s until 5.0 s and 0.5 s between 5.0 to 9.5 s). The inversions of 1.0 and 10 s were discarded due to the small number of inter-station paths (see Fig. S3, supplementary material). The final group velocity maps for selected periods are represented on Fig. S6 of the electronic supplementary material. Sensitivity kernels computed for the periods of interest indicate that the Rayleigh waves are mostly sensitive to structure down to about 10 km (Fig. S7, supplementary material).

5.3. 1-D depth inversion

To obtain the depth structure beneath the Fogo Island, we extracted the values of velocity, from the set of 2D group-velocity maps, for 608 points of the grid. In practical terms, we have, for each geographical point, a local dispersion curve. The further inversion of these curves enables the construction of a 1D S-wave velocity profile, as function of depth, for each node. To perform these inversions, we used the iterative linearized least-square inversion method of Herrmann and Ammon (2004) under the code surf96 (Herrmann, 2013). This algorithm iteratively perturbs a layered velocity model until a best fit between observed dispersion measurements and a synthetic dispersion curve is achieved.

Before starting with the inversion for each grid point it is necessary to choose an adequate initial velocity model. There exist 1D models calculated both for the Cape Verde Archipelago (e.g. Carvalho et al., 2019b;

Pim et al., 2008; Vales et al., 2014; Wilson et al., 2010) and for the individual islands (e.g. Lodge and Helffrich, 2006; Vinnik et al., 2012), yet most of them are not suitable to be used as starting model in this study due to the lack of resolution at crustal depths. In the absence of a reference starting model for the island, we decided to use the model proposed by Wilson et al. (2010). This velocity model is based on P-wave velocities obtained in a wide-angle refraction profile in the Archipelago of Cape Verde. A constant Vp/Vs ratio of 1.75 was used for all layers and the density values were taken from Wilson et al. (2010). The starting model was divided in 23 layers, the first six layers have a thickness of 0.5 km, and the remaining ones are 1 km thick.

The final model resolution can be strongly influenced by the damping and smoothing parameters, therefore we run different combinations of both parameters before computing the final inversions. We first tested the damping parameter by progressively increasing its value, starting from zero, while keeping fixed the smoothing parameter at 1. We determined that for damping values smaller than 1 the models present a better fit to the dispersion data. The smoothing factor was also tested, varying from 0.1 to 1, with and without weighing on specific layers. The inversion parameters were selected according to how well the final models fit the observed data. An example of the fitting between the model and the Rayleigh wave group velocity measurements can be seen in Fig. S8 (supplementary material). Finally, the depth inversion was performed in 25 iterations and the resultant 608 local Vs models together with the starting model (Wilson et al., 2010) are represented in Fig. 6.

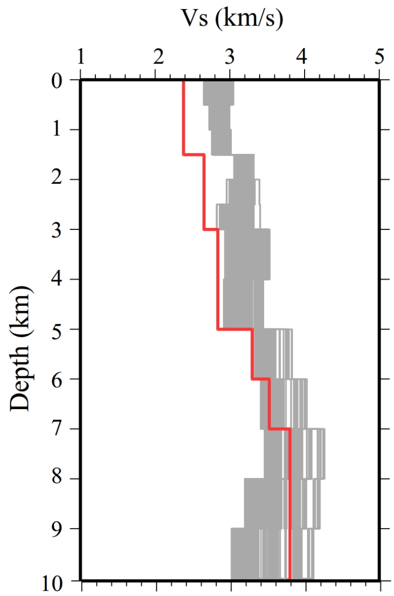

Figure 6: 1D S-wave velocity models derived for each grid node (grey lines) and the reference model obtained from Wilson et al. (2010) (red line).

5.4. 3D shear-wave velocity model

The 3D Vs model presented in Fig.7 in form of horizontal slices, for selected depths, shows the lateral velocity variation with respect to a depth-dependent average velocity over the first 10 km depth of the crust. The most striking feature of these maps is the well-defined separation between negative and positive velocity anomalies. In fact, the two anomalies appear clearly defined over the island: a prominent low-velocity anomaly in the north-eastern sector of the island, between 3.5 and 4.5 km of depth, and a high-velocity anomaly that extends to the remaining area of the island. Both anomalies persist in all maps, yet they become weaker (velocity becomes close to the average) as the depth increases.

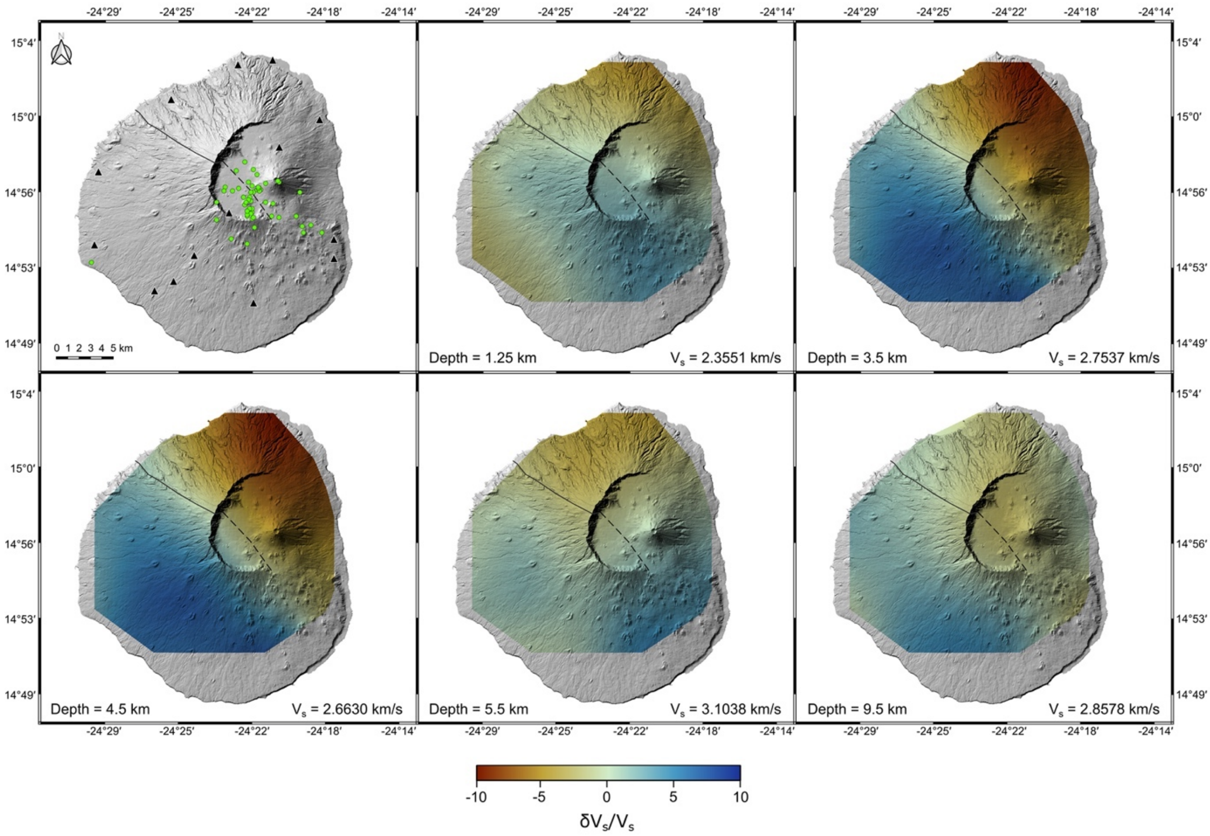

Figure 7: Map of Fogo Island with the seismic stations (triangles) and the seismic events detected during the 2014-2015 eruption (green dots) (top, left panel), plotted over hillshade topography of the island. Shear-wave velocity maps are presented for different depths (indicated in the bottom left). Velocity variations range from -10 per cent (red) to +10 percent (blue) with respect to a depth-dependent average velocity that is given at the bottom right of each panel.

Similarly, shear wave velocity profiles (Fig. 8) are illustrative of the differential velocity distribution beneath Fogo Island. These profiles show a shallow thick low velocity layer exhibiting velocities broadly between 2.2

and 2.8 km/s. It is directly located above a sharp increase in velocities at 5–6 km depth and down to 8–9 km depth, with values between 3.2 and 3.6 km/s, followed by yet another sharp decrease below 8–9 km depth to velocities within the 2.9–2.6 km/s range. This pattern is detected and consistent across the different profiles.

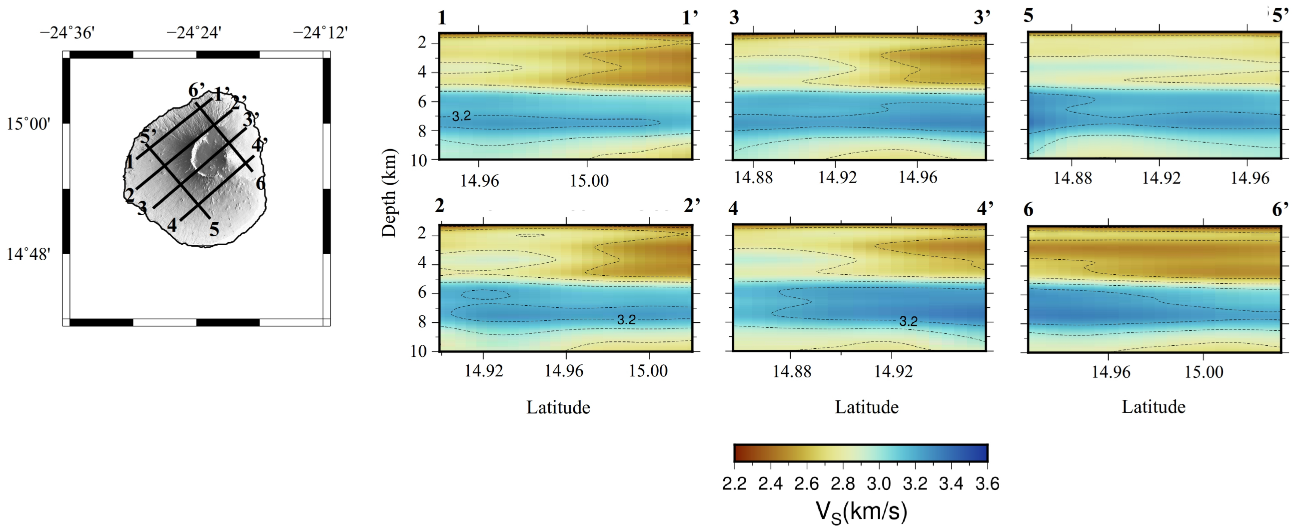

Figure 8: Shear-wave velocities along selected profiles on Fogo Island. Note the very distinct tabular high velocity zones at 3.5–4.5 km depth and at 5–9 km depth. The high velocity zone at 3.5-4.5 km depth is restricted to the south-western sector of the island.

Within the topmost layer, however, the lowest velocities are usually attained on the northeastern sector of the island, whilst the south-western attain consistently higher shear wave velocities. A more detailed look on these profiles shows the presence of a higher velocity body (up to 3.1 km/s) located between 3 and 4.5 km of depth, and exclusively on the southwestern sector of the island, not extending beyond the approximate location of the Galinheiros Fault (see Fig. 9). In a similar fashion, it is noticeable that the higher velocity layer detected in the middle of the profile (broadly between 5–9 km of depth) extends downwards to ~10 km along the southwesternmost sector of these profiles.

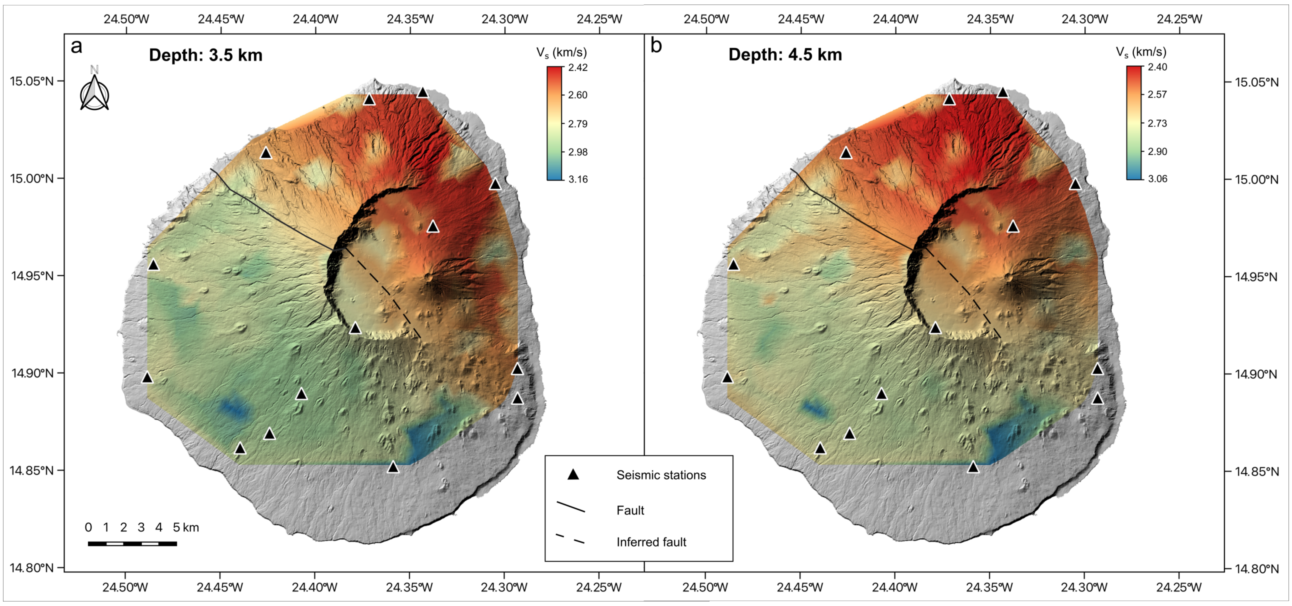

Figure 9: Shear-wave velocity maps for 3.5 and 4.5 km depth over hillshade topography of Fogo Island. The seismic stations are plotted using black triangles. Note the spatial agreement between the Galinheiros Fault and the two main zones of shear-wave velocities to the NE (low velocities) and SW (high velocities) of this fault.

6. Discussion

The ambient seismic noise technique allowed us to build EGFs between pairs of stations and to perform group velocity measurements over all inter-station paths. Following the 2D velocity tomography, the group-velocities obtained for each cell were inverted to obtain the first 3D shear-wave velocity model depicting the upper and middle crustal structure of Fogo Island.

The obtained shear-wave velocity models exhibit three main domains: (1) a largely asymmetric upper layer, above 5–6 km of depth, with lower velocities concentrated in the northeastern sector of the island and with a clear higher-velocity horizontal body at 3–4 km of depth in the southwestern sector of the island; (2) a higher-velocity layer located in between 5–6 km and 8–9 km (up to 10 km in the extreme southwest) of depth and exhibiting shear wave velocity values up to 3.6 km/s; and (3) a lower velocity layer below 8–9 km of depth, more pronounced beneath the northeastern sector of the island edifice. It must be stated that sharp increase in seismic velocities at ~5 km broadly corresponds to the base of the volcanic edifice, as inferred by the existing bathymetry and a seismic refraction profile in the vicinity of Fogo volcano, which places the top of the seafloor sediments (excluding the moat infill sediments) at 4-5 km, with the extrusive and intrusive oceanic crustal layers at, respectively, 5–7 and 7–13 km of depth (Pim et al., 2008; Wilson et al., 2010).

The presence of higher-velocity domains beneath both active and extinct ocean island volcanoes and other volcanic systems has been widely documented. For example, these have been detected beneath central volcanoes in Iceland (e.g. Gudmundsson et al., 1994; Brandsdóttir et al., 1997; Obermann et al., 2016; Jeddi et al., 2016), at Mt Etna, Italy (Chiarabba et al., 2000; Aloisi et al., 2002) as well as beneath Kilauea in Hawaii (Okubo et al., 1997) and Piton de la Fournaise (Brenguier et al., 2007; Mordret et al, 2015). In all these settings, such higher-velocity anomalies have been attributed to the presence of higher density, cooled intrusive magmatic bodies – such as sills, laccoliths, plutons, and old magma chambers - now composed of crystalline rocks and/or cumulates (Okubo et al., 1997, Brenguier et al., 2007; Paulatto et al., 2012; Shomali and Shirzad, 2015; Benediktsdóttir et al., 2017). Their presence has also been confirmed by combined seismic refraction and/or gravity data (e.g. Zucca et al., 1982; Gailler et al., 2009; Flinders et al., 2013; Gailler et al., 2010). Accordingly, we also interpret the higher velocities beneath Fogo as the seismic expression of pervasive sill and laccolith intrusions, now cooled, beneath the volcanic edifice and within the underlaying oceanic crust, and to a lesser extent, higher up within the volcanic edifice, the latter with a more asymmetric distribution, i.e. mostly concentrated beneath the southwestern sector of the island (see Fig. 10).

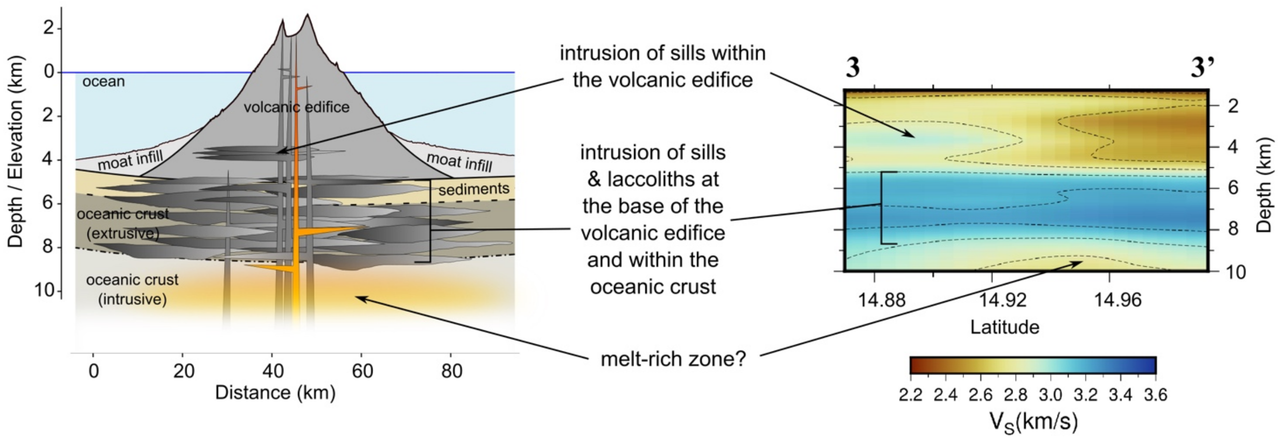

Figure 10: Conceptual SW–NE cross-section of Fogo Island down to ~10 km of depth, as interpreted by the shear-wave velocities along the same direction (see Fig. 9). In our opinion these velocities can be explained by the intrusion of sills and laccoliths preferentially within the sedimentary and extrusive part of the oceanic crust, in between 5 and 9 km of depth, and to a lesser extent also within the volcanic edifice, beneath the southwestern sector of the island and between 3.5 and 4.5 km of depth.

The preferential intrusion of sills and laccoliths beneath the volcanic edifice and mostly within the sedimentary and intrusive layers of the oceanic crust is to be expected, given that these horizons provide the ideal rigidity (between the soft sediments and the overlying volcanic edifice) and rheological conditions to the lateral intrusion of magmatic bodies (Menand, 2011; Galland et al., 2018). This interface appears to be shallower than the Moho, which is estimated to be ~12-14 km depth beneath Fogo Island (Lodge and Helffrich, 2006) and which represents another discontinuity where magma can preferentially be injected especially in intraplate settings as illustrated during the 2011-2012 unrest at El Hierro island (Benito-Saz et al., 2017). Petrological and geochemical studies of the 1995 and 1951 lava tend to confirm this trend of intrusions in the lower crust, with evidence suggesting the transient stalling of rising magma at depth ranging from 8 to 12 km, just above the Moho discontinuity (Hildner et al., 2011, 2012) and beneath what appears as a dense intrusive layer between 5 and 8 km depth. It is therefore conceivable that, over the time elapsed since the onset of Fogo's volcanism, the oceanic crust has been gradually modified by higher-density magmatic intrusions, which contributed to the present-day seismic velocities observed in this area. Moreover, significant crustal thickening by pervasive intrusion of sills and laccoliths beneath the island edifices has been widely reported in Cape Verde and even linked to significant local uplift trends experienced by some islands, such as Brava, Santiago and São Nicolau (Madeira et al., 2010; Ramalho et al., 2010a,b.c; Ramalho, 2011), as it has been in other archipelagos (Klügel et al, 2005; Klügel et al., 2015; Ramalho et al., 2015b; Ramalho et al., 2017). Our study therefore suggests that Fogo, despite being one the youngest islands in the archipelago and not yet exhibiting a particularly thickened crust (Lodge and Helffrich, 2006; Vinnik et al., 2012), is already underlain by a considerable amount of crystalline intrusive basement, responsible for the observed high velocities.

Similarly, this study highlighted the differential intrusion of sills within the volcanic edifice, mainly detected beneath the southwestern sector of Fogo. Effectively, the boundary between the two main zones of shear-wave velocities in the NE (lower-velocities) and SW (higher velocities) of Fogo at 3–4.5 km broadly coincides with the location of the Galinheiros normal fault. We therefore propose that the Galinheiros Fault could represent the surface expression of intrusive activity within the volcanic edifice (with uplift of the southwestern block relatively to the northeastern one), which took place sometime after ~120 ka (when the broad shield surface of the old volcanic edifice at Fogo was formed; Foeken et al., 2009) and prior to the Holocene when most of the volcanic activity at Pico do Fogo and Chã das Caldeiras took place. Again, the presence of sills shallow within the volcanic edifice, may have contributed to temporary magma stalling at very shallow levels, as inferred by petrological studies on the 2014-2015 lavas (Mata et al., 2017).

In contrast with the scenario described above, the lower velocities located beneath the northeastern sector of the island and within the island edifice (i.e. above 5 km) can be explained the presence of a largely unintruded, altered, and fluid-saturated volcanic sequence, i.e. represent parts of the volcanic edifice that have been unperturbed by sill and laccolith intrusions. Whilst higher-density, crystalline bodies contribute to higher seismic velocities, altered (e.g. the palagonitized hyaloclastites that compose the island pedestal) and fluid-saturated (seawater) sequences are conversely expected to result in slow(er) seismic velocities (Oheler et al., 2005). Profile 6-6' of Fig. 8 can thus be considered representative of the expected velocities of the volcanic edifice, prior to perturbations by the intrusion of (now) crystalline magmatic bodies.

Critically, these observations provide another line of evidence for the absence of any sizable shallow (i.e. within the island edifice) magma chambers at Fogo, either ancient or recent, in agreement with previous geophysical and petrological studies. Such reservoir, if present, would result in a marked decrease in seismic velocities within the core of the edifice, a feature that is not supported by our tomographic observations.

Finally, the sharp shear-wave velocity reduction below 8-9 km of depth might be explained by a hotter and possibly melt-rich zone beneath the volcano. Alternatively, it could be explained by a significantly altered/serpentinized crust, which would result in lower velocities. This lower velocity anomaly, however, is close to the limit of resolution of our model, and therefore will need to be confirmed by further studies.

7. Conclusions

This contribution illustrates how ambient noise tomography applied to low or almost non-existent seismic activity can be an effective and useful technique with great potential in constraining the main volcanic structures. This study presents for the first time a 3D shear-wave velocity model for the island of Fogo. Our main goal was to provide new insights into the volcano internal and upper crustal structure and tectonic features, but also to contribute to a better understanding of both seismic events and volcanic activity, i.e shedding light into the location of earthquake hypocenters and the structural discontinuities that may influence transient magma stalling on its way to the surface. Our study effectively shows that Fogo Island rests on a layer of higher Vs seismic velocities, between 5-6 km and 8-9 km, interpreted as the result of pervasive sill and laccolith intrusions at the base of the edifice and within the oceanic crust, and that the edifice is also differentially intruded by sills at shallower levels, as suggested by a clear horizontal layer of higher seismic velocities at 3-4 km and restricted to the southwestern sector of the edifice. The intrusion of these magmatic bodies at shallow levels may also be responsible for long-term surface deformation, materialized by the Galinheiros normal fault, and is compatible with petrological studies that infer transient magma stalling at both depth domains. Our study also confirms that there is no shallow magma chamber, ancient or recent, at Fogo volcano, thus providing an important contribution to our stepwise knowledge of this volcanic system.

ACKNOWLEDGEMENTS

This study is a contribution to projects FIRE (Ref. PTDC/GEO-GEO/1123/2014), SIGHT (Ref. PTDC/CTA-GEF/30264/2017) and RESTLESS (Ref. PTDC/CTAGEF/6674/2020). This work is also developed in the framework of the Portuguese Fundação para a Ciência e Tecnologia (FCT) UIDB/50029/2020 - Instituto Dom Luiz. Joana Carvalho was supported by the FCT projects PTDC/CTA-GEF/30264/2017 and PTDC/CTAGEF/6674/2020. Stéphanie Dumont acknowledges FCT and the European Union (UE) for their financial support through the postdoctoral fellowship SFRH/BPD/117714/2016, co-financed by the Ministério da Ciência, Tecnologia e Ensino Superior (MCTES), Fundo Social Europeu (FSE), and Programa Operacional Regional Centro (Centro 2020) as well as her FCT-funded contract 2021.00876.CEECIND. Most figures were made using GMT - Generic Mapping Tools (Wessel et al., 2013).

REFERENCES

Acevedo, J., Fernández-Viejo, G., Llana-Fúnez, S., López-Fernández, C., & Olona, J. (2019). Ambient noise tomography of the southern sector of the Cantabrian Mountains, NW Spain. *Geophys J Int*, *219*(1), 479–495. https://doi.org/10.1093/gji/ggz308

Aiuppa, A., Bitetto, M., Rizzo, A. L., Viveiros, F., Allard, P., Frezzotti, M. L., ... & Zanon, V. (2020). The fumarolic CO_2 output from Pico do Fogo Volcano (Cape Verde). *Italian Journal of Geosciences*, *139*(3), 325-340.

Aloisi, M., Cocina, O., Neri, G., Orecchio, B., Privitera, E., 2002. Seismic tomography of the crust underneath the Etna volcano, Sicily. *Phys. Earth Planet. Int*. 134, 139–155.

Alonso, M., Pérez, N. M., Padrón, E., Hernández, P. A., Melián, G. V., Sumino, H., ... & Pereira, J. M. (2021). Changes in the thermal energy and the diffuse ^3He and ^4He degassing prior to the 2014–2015 eruption of Pico do Fogo volcano, Cape Verde. *J. Volcanol. Geotherm. Res.*, 416, 107271.

Amelung, F. and S. Day (2002). InSar observation of the 1995 Fogo, Cape Verde, eruption: Im- plication for the effects of collapse events upon island volcanoes. *Geophys. Res. Lett.*, Vol. 29, 12,10.1029/2001GL013760.

Benediktsdóttir, Á., Gudmundsson, Ó., Brandsdóttir, B., & Tryggvason, A. (2017). Ambient noise tomography of Eyjafjallajökull volcano, Iceland. *J. Volcanol. Geotherm. Res.*, *347*, 250–263. https://doi.org/10.1016/j.jvolgeores.2017.09.017

Benito-Saz, M. A., Parks, M. M., Sigmundsson, F., Hooper, A., & García-Cañada, L. (2017). Repeated magmatic intrusions at El Hierro Island following the 2011–2012 submarine eruption. J. Volcanol. Geotherm. Res., 344, 79-91.

Bernard-Griffiths, J., Cantagrel, J.M., Alves, C., Mendes, F., Serralheiro, A., and Macedo, J. (1975) Geochronologie: donnés radiometriques potassium-argon sur quelques formations magmatiques des îlles de l'archipel du Cap Vert CR: Académie des Sciences, Paris, v. 280, p. 2429– 2432.

Brandsdóttir, B., Menke, W., Einarsson, P., White, R., Staples, R., 1997. Färoe-Iceland Ridge Experiment 2. Crustal structure of the Krafla central volcano. *J. Geophys. Res*. 102, 7867–7886.

Brenguier, F., Shapiro, N. M., Campillo, M., Nercessian, A., & Ferrazzini, V. (2007). 3-D surface wave tomography of the Piton de la Fournaise volcano using seismic noise correlations. *Geophys. Res. Lett.*, *34*(2), 2–6. https://doi.org/10.1029/2006GL028586

Brum da Silveira, A., Madeira, J., Serralheiro, A. (1997a). A estrutura da Ilha do Fogo, Cabo Verde, in *A Erupção Vulcânica de 1995 na Ilha do Fogo, Cabo Verde* (Publ. IICT, Lisboa, Portugal), pp. 63–78. *In Portuguese*.

Brum da Silveira, A., Madeira, J., Serralheiro, A., Torres, P.C., Silva, L.C., Mendes, M.H. (1997b). O controlo estrutural da erupção de Abril de 1995 na Ilha do Fogo, Cabo Verde, in *A Erupção Vulcânica de 1995 na Ilha do Fogo, Cabo Verde* (Publ. IICT, Lisboa, Portugal), pp. 51–61. *In Portuguese*.

Campillo, M., & Paul, A. (2003). Long-range correlations in the diffuse seismic coda. *Science*, *299*(5606), 547-549.

Cappello, A., Ganci, G., Calvari, S., Pérez, N. M., Hernández, P. A., Silva, S. V., ... & Del Negro, C. (2016). Lava flow hazard modeling during the 2014–2015 Fogo eruption, Cape Verde. *J. Geophys. Res. B: Solid Earth*, 121(4), 2290-2303.

Carracedo, J.C., Perez-Torrado, F. J., Rodriguez-González, A., Paris, R., Troll, V. R., & Barker, A. K. (2015). Volcanic and structural evolution of Pico do Fogo, Cape Verde. *Geology Today*, *31*(4), 146–152.

https://doi.org/10.1111/gto.12101

Carvalho, J., Bonadio, R., Silveira, G., Lebedev, S., Mata, J., Arroucau, P., Meier, T., & Celli, N. L. (2019b). Evidence for high temperature in the upper mantle beneath Cape Verde archipelago from Rayleigh-wave phase-velocity measurements. *Tectonophysics*, *770*, 228225. https://doi.org/10.1016/j.tecto.2019.228225

Carvalho, J., Silveira, G., Kiselev, S., Custódio, S., Ramalho, R.S., Stutzmann, E. & Schimmel, M. (2022). Lower crust and uppermost mantle structure of Cape Verde from ambient noise tomography. *Geophys. J. Int.* 231 (2), November 2022, 1421–1433. https://doi.org/10.1093/gji/ggac254

Celli, N. L., Lebedev, S., Schaeffer, A. J., Ravenna, M., & Gaina, C. (2020). The upper mantle beneath the South Atlantic Ocean, South America and Africa from waveform tomography with massive data sets. *Geophys. J. Int.*, *221*(1), 178–204. https://doi.org/10.1093/gji/ggz574

Corela, C., Silveira, G., Matias, L., Schimmel, M., & Geissler, W. H. (2017). Ambient seismic noise tomography of SW Iberia integrating seafloor- and land-based data. *Tectonophysics*, *700–701*, 131–149. https://doi.org/10.1016/j.tecto.2017.02.012

Cornu, M. N., Paris, R., Doucelance, R., Bachèlery, P., Bosq, C., Auclair, D., ... & Guillou, H. (2021). Exploring the links between volcano flank collapse and the magmatic evolution of an ocean island volcano: Fogo, Cape Verde. Scientific Reports, 11(1), 1-12.

Chiarabba, C., Amato, A., Boschi, E., Barberi, F., 2000. Recent seismicity and tomographic modeling of the Mount Etna plumbing system. J. Geophys. Res. 105, 10923–10938.

Day, S.J., Heleno da Silva, S. I. N. & Fonseca, J. F. B. D. (1999) - A past giant lateral collapse and present-day flank instability of Fogo, Cape Verde Islands. J. Volcanol. Geotherm. Res., 94(1-4), 191-218.

Dumont, S., Silveira, G., Custódio, S., Lopes, F., Le Mouël, J.-L., Gouhier, M., & Guéhenneux, Y. (2021). Response of Fogo volcano (Cape Verde) to lunisolar gravitational forces during the 2014–2015 eruption. *Phys. Earth Planet. Inter.*, *312*, 106659. https://doi.org/10.1016/j.pepi.2021.106659

Dziewonski, A., Bloch, S., & Landisman, M. (1969). A technique for the analysis of transient seismic signals. Bull. Seismol. Soc. Am., 59(1), 427–444.

Faria, B., & Fonseca, J. F. B. D. (2014). Investigating volcanic hazard in Cape Verde Islands through geophysical monitoring: network description and first results. *Nat. Hazards Earth Syst. Sci.*, *14*(2), 485–499. https://doi.org/10.5194/nhess-14-485-2014

Flinders, A.F., Ito, G., Garcia, M.O., Sinton, J.M., Kauahikaua, J. and Taylor, B., 2013. Intrusive dike complexes, cumulate cores, and the extrusive growth of Hawaiian volcanoes. Geophys. Res. Lett. , 40(13), pp.3367-3373.

Foeken, J.P., Day, S. and Stuart, F.M., 2009. Cosmogenic 3He exposure dating of the Quaternary basalts from Fogo, Cape Verdes: implications for rift zone and magmatic reorganisation. Quaternary Geochronology, 4(1), pp.37-49.

Fonseca, J. F. B. D., Faria, B. V. E., Trindade, J., Cruz, G., Chambel, A., Silva, F. M., Pereira, R. L., & Vazão, T. (2013). “Last miles” challenges to in situ volcanic data transmission. *Nat. Hazards Earth Syst. Sci.*, *13*(12), 3419–3428. https://doi.org/10.5194/nhess-13-3419-2013

French, S. W., & Romanowicz, B. A. (2014). Whole-mantle radially anisotropic shear velocity structure from spectral-element waveform tomography. *Geophys. J. Int. 199*(3), 1303–1327 https://doi.org/10.1093/gji/ggu334

Gailler, L. S., Lénat, J. F., Lambert, M., Levieux, G., Villeneuve, N., & Froger, J. L. (2009). Gravity structure of Piton de la Fournaise volcano and inferred mass transfer during the 2007 crisis. J. Volcanol. Geotherm.

Res., 184(1-2), 31-48.

Gailler, L. S., & Lénat, J. F. (2010). Three-dimensional structure of the submarine flanks of La Réunion inferred from geophysical data. J. Geophys. Res. B: Solid Earth, 115(B12).

Galland, O., Bertelsen, H. S., Eide, C. H., Guldstrand, F., Haug, Ø. T., Leanza, H. A., ... & Spacapan, J. B. (2018). Storage and transport of magma in the layered crust—Formation of sills and related flat-lying intrusions. In Volcanic and igneous plumbing systems (pp. 113-138). Elsevier.

Goldstein, P., and A. Snoke (2005). SAC availability for the IRIS community, Incorporated Research Institutions for Seismology Newsletter, 7 (UCRL-JRNL-211140).

González, P. J., Bagnardi, M., Hooper, A. J., Larsen, Y., Marinkovic, P., Samsonov, S. V., & Wright, T. J. (2015). The 2014–2015 eruption of Fogo volcano: Geodetic modeling of Sentinel-1 TOPS interferometry. *Geophys. Res. Lett.* , 42(21), 9239-9246.

Gudmundsson, O., Brandsdottir, B., Menke, W., Sigvaldason, G., 1994. The crustal magma chamber of the Katla volcano in south Iceland revealed by 2-D seismic undershooting. *Geophys. J. Int.* 119 (1), 277–296.

Hable, S., Sigloch, K., Stutzmann, E., Kiselev, S., & Barruol, G. (2019). Tomography of crust and lithosphere in the western Indian Ocean from noise cross-correlations of land and ocean bottom seismometers. *Geophys. J. Int.*, *219*(2), 924–944. https://doi.org/10.1093/gji/ggz333

Haned, A., Stutzmann, E., Schimmel, M., Kiselev, S., Davaille, A., & Yelles-Chaouche, A. (2016). Global tomography using seismic hum. *Geophys J Int*, *204*(2), 1222–1236. https://doi.org/10.1093/gji/ggv516

Heleno da Silva, S. I. N., Day, S. J., & Fonseca, J. F. B. D. (1999). Fogo Volcano, Cape Verde Islands: seismicity-derived constraints on the mechanism of the 1995 eruption. *J. Volcanol. Geotherm. Res.*, *94*(1–4), 219–231. https://doi.org/10.1016/S0377-0273(99)00104-3

Helffrich, G., Faria, B., Fonseca, J. F., Lodge, A., & Kaneshima, S. (2010). Transition zone structure under a stationary hot spot: Cape Verde. *Earth Planet. Sci. Lett.*, *289*(1-2), 156-161.

Herrmann, R. B (2013). Computer programs in seismology: an evolving tool for instruction and research. *Seismol Res Lett* 84:1081–1088. https://doi.org/10.1785/0220110096

Herrmann, R.B. & Ammon, C.J., 2004. Surface waves, receiver functions and crustal structure. *Computer programs in seismology, version*, *3*, 30.

Hildner, E., Klügel, A., & Hauff, F. (2011). Magma storage and ascent during the 1995 eruption of Fogo, Cape Verde Archipelago. *Contributions to Mineralogy and Petrology*, *162*(4), 751–772. https://doi.org/10.1007/s00410-011-0623-6

Hildner, E., Klügel, A., & Hansteen, T. H. (2012). Barometry of lavas from the 1951 eruption of Fogo, Cape Verde Islands: Implications for historic and prehistoric magma plumbing systems. *J. Volcanol. Geotherm. Res.*, *217–218*, 73–90. https://doi.org/10.1016/j.jvolgeores.2011.12.014

Jaxybulatov, K., Koulakov, I., Ibs-von Seht, M., Klinge, K., Reichert, C., Dahren, B. & Troll, V.R., 2011. Evidence for high fluid/melt content beneath Krakatau volcano (Indonesia) from local earthquake tomography, *J. Volc. Geotherm. Res.*, 206(3–4), 96–105.

Jeddi, Z., Tryggvason, A., Gudmundsson, O. (2016). The Katla Volcanic system imaged using local earthquakes recorded with a temporary seismic network. *J. Geophys. Res*. 102

Jeddi, Z., Gudmundsson, O., & Tryggvason, A. (2017). Ambient-noise tomography of Katla volcano, south Iceland. *J. Volcanol. Geotherm. Res.*, *347*, 264–277. https://doi.org/10.1016/j.jvolgeores.2017.09.019

Jenkins, S. F., Day, S. J., Faria, B. V. E., & Fonseca, J. F. B. D. (2017). Damage from lava flows: insights from the 2014–2015 eruption of Fogo, Cape Verde. *J. Appl. Volcanol.*, *6*(1). https://doi.org/10.1186/s13617-017-0057-6

Klügel, A., Hansteen, T.H. and Galipp, K., (2005). Magma storage and underplating beneath Cumbre Vieja volcano, la Palma (Canary Islands). *Earth Planet. Sci. Lett.*, 236(1-2), pp.211-226.

Klügel, A., Longpré, M.A., García-Cañada, L. and Stix, J. (2015). Deep intrusions, lateral magma transport and related uplift at ocean island volcanoes. *Earth Planet. Sci. Lett.*, 431, pp.140-149.

Klügel, A., Day, S., Schmid, M., & Faria, B. (2020). Magma Plumbing During the 2014–2015 Eruption of Fogo (Cape Verde Islands). *Front. Earth Sci.*, *8*(June). https://doi.org/10.3389/feart.2020.00157

Leva, C., Rümpker, G., Link, F., & Wölbern, I. (2019). Mantle earthquakes beneath Fogo volcano, Cape Verde: Evidence for subcrustal fracturing induced by magmatic injection. *J. Volcanol. Geotherm. Res.*, *386*, 106672. https://doi.org/10.1016/j.jvolgeores.2019.106672

Leva, C., Rümpker, G., & Wölbern, I. (2021). Multi-array analysis of volcano-seismic signals at Fogo and Brava, Cape Verde. *Solid Earth Discuss.*, May 1–26. https://doi.org/10.5194/se-2021-52

Levshin, A.L., Yanovskaya, T.B., Lander, A.V., Bukchin,B.G., Barmin,M.P., Ratnikova, L.I. & Its, E.N., 1989. Seismic Surface Waves in a Laterally Inhomogeneous Earth, Kluwer Academic Publishers

Liu, X., & Zhao, D. (2014). Seismic evidence for a mantle plume beneath the Cape Verde hotspot. *Int. Geol. Rev., 56*(10), 1213–1225. https://doi.org/10.1080/00206814.2014.930720

Liu, X., & Zhao, D. (2021). Seismic evidence for a plume-modified oceanic lithosphere–asthenosphere system beneath Cape Verde. *Geophys J Int*, *225*(2), 872–886. https://doi.org/10.1093/gji/ggab012

Lodge, A., & Helffrich, G. (2006). Depleted swell root beneath the Cape Verde Islands. *Geology*, *34*(6), 449. https://doi.org/10.1130/G22030.1

Maccaferri, F., Richter, N. & Walter, T.R. The effect of giant lateral collapses on magma pathways and the location of volcanism. *Nat Commun* 8, 1097 (2017). https://doi.org/10.1038/s41467-017-01256-2

Madeira, J.; Mata, J.; Mourão, C.; Brum da Silveira, A.; Martins, S.; Ramalho, R.; Hoffmann; D. Volcano-stratigraphic and structural evolution of Brava Island (Cape Verde) based on 40 Ar/39Ar, U-Th and field constraints, *J. Volcanol. Geotherm. Res.* (2010), Vol 196, 219-235.

Marques, F. O., Hildenbrand, A., Victória, S. S., Cunha, C., and Dias, P. (2019). Caldera or flank collapse in the Fogo volcano? What age? Consequences for risk assessment in volcanic islands. *J. Volcanol. Geotherm. Res*. 388:106686. doi: 10.1016/j.jvolgeores.2019.106686

Martínez-Moreno, F. J., Monteiro Santos, F. A., Madeira, J., Pous, J., Bernardo, I., Soares, A., Esteves, M., Adão, F., Ribeiro, J., Mata, J., & Brum da Silveira, A. (2018). Investigating collapse structures in oceanic islands using magnetotelluric surveys: The case of Fogo Island in Cape Verde. *J. Volcanol. Geotherm. Res.*, *357*, 152–162. https://doi.org/10.1016/j.jvolgeores.2018.04.028

Mata, J., Martins, S., Mattielli, N., Madeira, J., Faria, B., Ramalho, R. S., Silva, P., Moreira, M., Caldeira, R., Moreira, M., Rodrigues, J., & Martins, L. (2017). The 2014–15 eruption and the short-term geochemical evolution of the Fogo volcano (Cape Verde): Evidence for small-scale mantle heterogeneity. *Lithos*, *288–289*, 91–107. https://doi.org/10.1016/j.lithos.2017.07.001

Melián, G. V, Hernández, P. A., Pérez, N. M., Asensio-Ramos, M., Padrón, E., Alonso, M., Padilla, G. D., Barrancos, J., Sortino, F., Sumino, H., Rodríguez, F., Amonte, C., Silva, S., Cardoso, N., & Pereira, J. M. (2021). Insights from Fumarole Gas Geochemistry on the Recent Volcanic Unrest of Pico do Fogo, Cape Verde. *Front. Earth Sci.*, *9* (November 2008), 12754. https://doi.org/10.3389/feart.2021.631190

Menand, T., 2011. Physical controls and depth of emplacement of igneous bodies: A review. *Tectonophysics*, 500(1-4), pp.11-19.

Montelli, R., Nolet, G., Dahlen, F. A., & Masters, G. (2006). A catalogue of deep mantle plumes: New results from finite frequency tomography. *Geochem. Geophys. Geosyst.*, *7*(11). https://doi.org/10.1029/2006GC001248

Mordret, A., Rivet, D., Landès, M., & Shapiro, N. M. (2015). Three-dimensional shear velocity anisotropic model of Piton de la Fournaise Volcano (La Réunion Island) from ambient seismic noise. J. Geophys. Res. B: Solid Earth, 120(1), 406-427.

Munhá J. M., M. H. Mendes, T. Palácios, L. C. Silva e P. C. Torres (1997). Petrologia e geoquímica da erupção de 1995 e de outras lavas históricas na ilha do Fogo, Cabo Verde. In Rafega et al. (Eds.): A Erupção Vulcânica de 1995 na Ilha do Fogo, Cabo Verde. Instituto de Investigação Científica Tropical, Lisboa. *In portuguese*

Nuñez, E., Schimmel, M., Stich, D., & Iglesias, A. (2019). Crustal Velocity Anomalies in Costa Rica from Ambient Noise Tomography. *Pure Appl. Geophys.* https://doi.org/10.1007/s00024-019-02315-z

Obermann, A., Lupi, M., Mordret, A., Jakobsdóttir, S. S., & Miller, S. A. (2016). 3D-ambient noise Rayleigh wave tomography of Snæfellsjökull volcano, Iceland. *J. Volcanol. Geotherm. Res.*, *317*, 42–52. https://doi.org/10.1016/j.jvolgeores.2016.02.013

Oehler, J.-F., B. van Wyk de Vries, and P. Labazuy (2005), Landslides and spreading of oceanic hot-spot and arc shield volcanoes on Low Strength Layers (LSLs): An analogue modeling approach, J. Volcanol. Geotherm. Res., 144(1), 169–189.

Okubo, P., Benz, H., Chouet, B. (1997). Imaging the crustal magma sources beneath Mauna Loa and Kilauea volcanoes, Hawaii. *Geology* 25, 867–870.

Paulatto, M., Annen, C., Henstock, T.J., Kiddle, E., Minshull, T.A., Sparks, R., Voight, B. (2012). Magma chamber properties from integrated seismic tomography and thermal modeling at Montserrat. *Geochem. Geophys. Geosyst*. 13 (1).

Pim, J., Peirce, C., Watts, A. B., Grevemeyer, I., & Krabbenhoeft, A. (2008). Crustal structure and origin of the Cape Verde Rise. *Earth Planet. Sci. Lett.*, *272*(1–2), 422–428. https://doi.org/10.1016/j.epsl.2008.05.012

Ramalho, R.; Helffrich, G.; Cosca, M.; Vance, D.; Hoffmann, D.; Schmidt, D.N. (2010a) Episodic hotspot swell growth inferred from variable uplift from the Cape Verde hot spot Islands. *Nature Geoscience*, Vol3, 774-777.

Ramalho, R.; Helffrich, G.; Cosca, M.; Vance, D.; Hoffmann, D.; Schmidt, D.N. (2010b) Vertical movements of ocean island volcanoes: insights from a stationary plate. *Marine Geology*, vol. 275, pp 84-95.

Ramalho, R.; Helffrich, G.; Schmidt, D.N.; Vance, D. (2010c) Tracers of uplift and subsidence in the Cape Verde Archipelago. *J. Geol. Soc. London*. V.167, pp 519-538.

Ramalho, R. A. (2011). Building the Cape Verde islands. *In Springer Thesis*.

Ramalho, R. S., Winckler, G., Madeira, J., Helffrich, G. R., Hipólito, A., Quartau, R., ... & Schaefer, J. M. (2015a). Hazard potential of volcanic flank collapses raised by new megatsunami evidence. *Science advances*, 1(9), e1500456.

Ramalho, R.; Brum da Silveira, A.; Fonseca, P.; Madeira; J. Cosca, M.; Cachão, M.; Fonseca, M.; Prada, S. (2015b) The emergence of volcanic oceanic islands on a slow-moving plate: the example of Madeira Island, NE Atlantic. *Geochem. Geophys. Geosyst.*, 16, 522–537.

Ramalho, R.S., Helffrich, G., Madeira, J., Cosca, M., Thomas, C., Quartau, R., Hipólito, A., Rovere, A., Hearty, P.J. and Ávila, S.P., (2017). Emergence and evolution of Santa Maria Island (Azores)—The conundrum of uplifted islands revisited. Bulletin, 129(3-4), pp.372-390.

Rawlinson, N., & Sambridge, M. (2005). The fast marching method: an effective tool for tomographic imaging and tracking multiple phases in complex layered media. *36*(4), 341–350.

Rawlinson, N., Reading, A. M., & Kennett, B. L. (2006). Lithospheric structure of Tasmania from a novel form of teleseismic tomography. *J. Geophys. Res. B: Solid Earth*, *111*(B2).

Ribeiro, O. (1960). A Ilha do Fogo e as suas Erupções. Junta de Investigações do Ultramar, Lisbon. *In Portuguese*

Samrock, L. K., Wartho, J. A. and Hansteen, T. H. (2019). 40Ar-39Ar geochronology of the active phonolitic Cadamosto Seamount, Cape Verde. *Lithos*, 344, 464-481.

Sánchez-Pastor, P., Obermann, A., Reinsch, T., Ágústsdóttir, T., Gunnarsson, G., Tómasdóttir, S., Hjörleifsdóttir, V., Hersir, G. P., Ágústsson, K., & Wiemer, S. (2021). Imaging high-temperature geothermal reservoirs with ambient seismic noise tomography, a case study of the Hengill geothermal field, SW Iceland. *Geothermics*, *96*(July), 102207. https://doi.org/10.1016/j.geothermics.2021.102207

Schaeffer, A. J., & Lebedev, S. (2015). Global heterogeneity of the lithosphere and underlying mantle: A seismological appraisal based on multimode surface-wave dispersion analysis, shear-velocity tomography, and tectonic regionalization. In *The Earth's heterogeneous mantle* (pp. 3–46).

Schimmel, M., Stutzmann, E., Ardhuin, F., & Gallart, J. (2011). Polarized Earth's ambient microseismic noise. *Geochem. Geophys. Geosyst.*, *12*(7), n/a-n/a. https://doi.org/10.1029/2011GC003661

Schimmel, Martin. (1999). Phase cross-correlations: Design, comparisons, and applications. *Bull. Seismol. Soc. Am.*, *89*(5), 1366–1378.

Schimmel, M., Stutzmann, E., Ventosa, S., (2017). Measuring Group Velocity in Seismic Noise Correlation Studies Based on Phase Coherence and Resampling Strategies, IEEE Transactions on Geoscience and Remote Sensing, 55(4), pp. 1928-1935. DOI: 10.1109/TGRS.2016.2631445.

Shapiro, N. M., & Campillo, M. (2004). Emergence of broadband Rayleigh waves from correlations of the ambient seismic noise. *Geophys. Res. Lett. 31*(7), n/a-n/a. https://doi.org/10.1029/2004GL019491

Shomali, Z. H., & Shirzad, T. (2015). Crustal structure of Damavand volcano, Iran, from ambient noise and earthquake tomography. *J. Seismolog.*, *19*(1), 191–200. https://doi.org/10.1007/s10950-014-9458-8

Silveira, G., Dias, N.A., Kiselev, S., Stutzmann, E., Custódio, S. and Schimmel., M. (2022) Imaging the crust and uppermost mantle structure of Portugal (West Iberia) with seismic ambient noise. *Geophys. J. Int.* 230(2), 1106-1120. https://doi.org/10.1093/gji/ggac106.

Stankiewicz, J., Ryberg, T., Haberland, C., Fauzi, & Natawidjaja, D. (2010). Lake Toba volcano magma chamber imaged by ambient seismic noise tomography. *Geophys. Res. Lett. 37*(17), n/a-n/a. https://doi.org/10.1029/2010GL044211

Tanaka, S., Hamaguchi, H., Nishimura, T., Yamawaki, T., Ueki, S., Nakamichi, H., ... & Aizawa, K. (2002). Three-dimensional P-wave velocity structure of Iwate volcano, Japan from active seismic survey. *Geophys. Res. Lett.* ,*29*(10), 59-1.

Torres, P. C., Madeira, J., Silva, L. C., Brum da Silveira, A., Serralheiro, A. Mota Gomes, A. (1998). Carta geológica da Ilha do Fogo (República de Cabo Verde): erupções históricas e formações enquadrantes. Geological Map Lattex, (1 sheet at 1:25.000 scale).

Torres, P., Silva, L., Munhá, J., Caldeira, R., Mata, J., & Tassinari, C. C. (2010). Petrology and geochemistry of lavas from Sal Island: implications for the variability of the Cape Verde magmatism. *Comunicações Geológicas*.

Vales, D., Dias, N. A., Rio, I., Matias, L., Silveira, G., Madeira, J., Weber, M., Carrilho, F., & Haberland, C.

(2014). Intraplate seismicity across the Cape Verde swell: A contribution from a temporary seismic network. *Tectonophysics*, *636*, 325–337. https://doi.org/10.1016/j.tecto.2014.09.014

Vinnik, L., Silveira, G., Kiselev, S., Farra, V., Weber, M., & Stutzmann, E. (2012). Cape Verde hotspot from the upper crust to the top of the lower mantle. *Earth Planet. Sci. Lett.*, *319–320*, 259–268. https://doi.org/10.1016/j.epsl.2011.12.017

Weber, M. Silveira, G. and Schulze, A. (2007): The COBO/CV-PLUME temporary seismic network. GFZ Data Services. Other/Seismic Network. doi:10.14470/4N7552467332.

Wessel, P., W. H. Smith, R. Scharroo, J. Luis, and F. Wobbe (2013). Generic Mapping Tools: Improved version released, Eos Trans. AGU 94, no. 45, 409–410.

Wilson, D. J., Peirce, C., Watts, A. B., Grevemeyer, I., & Krabbenhoeft, A. (2010). Uplift at lithospheric swells - I: Seismic and gravity constraints on the crust and uppermost mantle structure of the Cape Verde mid-plate swell. *Geophys J Int*, *182*(2), 531–550. https://doi.org/10.1111/j.1365-246X.2010.04641.x

Worsley, P. (2015). Physical geology of the Fogo volcano (Cape Verde Islands) and its 2014-2015 eruption. *Geology Today*, *31*(4), 153–159. https://doi.org/10.1111/gto.12102

Yao, H., R. D. van der Hilst, and M. V. De Hoop (2006). Surface-wave array tomography in SE Tibet from ambient seismic noise and two-station analysis—I. Phase velocity maps, Geophys. J. Int. 166, 732–744.

Zucca, J.J., Hill, D.P. and Kovach, R.L. (1982). Crustal structure of Mauna Loa volcano, Hawaii, from seismic refraction and gravity data. Bull. Seismol. Soc. Am., 72(5), pp.1535-1550.